applied sciences

MDPI

Article

Research on Nonlinear Vibration Characteristics of Internal Beveloid Gear Transmission System

Jianmin Wen, Chenqi Fu, Hong Zhang and Bindi You *

School of Ocean Engineering, Harbin Institute of Technology, Weihai 264209, China; wenjm@hit.edu.cn (J.W.); fu_chenqi@163.com (C.F.); zhang.h1604@gmail.com (H.Z.)
* Correspondence: youbindi@hitwh.edu.cn

Abstract: The internal beveloid gear has good scientific research value and a broad application field. However, there is a lack of research on the nonlinear vibration characteristics of internal beveloid gears. The present study establishes a nonlinear vibration model that takes into account axial vibration, gear torsional vibration, and radial support vibration. The effects of various excitation parameters on the vibration characteristics of the gear transmission system are analyzed and computed using the Runge–Kutta method. After analyzing the dynamic model of the gear pair using numerical methods, the harmonic balance method is employed to obtain the theoretical analytical solution for a single−stage gear. The obtained results are compared with the velocity and acceleration time−domain response curves obtained from the numerical method, and they show excellent agreement.

Keywords: beveloid gears; Runge–Kutta method; nonlinear vibration; harmonic balance method

check for updates

Citation: Wen, J.; Fu, C.; Zhang, H.; You, B. Research on Nonlinear Vibration Characteristics of Internal Beveloid Gear Transmission System. *Appl. Sci.* **2023**, *13*, 12463. https://doi.org/10.3390/app132212463

Academic Editor: Jean-Jacques Sinou

Received: 20 October 2023
Revised: 9 November 2023
Accepted: 9 November 2023
Published: 17 November 2023

Copyright: © 2023 by the authors. Licensee MDPI, Basel, Switzerland. This article is an open access article distributed under the terms and conditions of the Creative Commons Attribution (CC BY) license (https://creativecommons.org/licenses/by/4.0/).

1. Introduction

As technology advances, gear transmission mostly moves in the directions of greater bearing capacity, increased stability, reduced vibration and noise, and exquisite structure [1]. Theoretically, beveloid gears offer a type of precision transmission with adjustable backlash [2]. Beveloid gears are advantageous for transmitting tiny tilt angles because they may adapt their design parameters to suit various gear transmission circumstances. The backlash may be efficiently adjusted by shifting the axial position of the gear teeth, according to some studies, which enhances the transmission's precision [3]. In some circumstances, the gear system's vibration and noise can have a significant negative impact [4]. In order to provide a theoretical foundation for the ongoing development of gear system vibration reduction and noise reduction technology, it is crucial to study the vibration characteristics of beveloid gears and analyze their nonlinear vibration characteristics.

Purkiss studied the gear teeth's meshing conditions in 1956 and provided a technique for machining external beveloid gears using a basic machine tool [5]. Mitome et al. thoroughly examined and analyzed the gear hobbing technique of beveloid gears in order to advance beveloid gears from theory to practice [6,7]. Zhao Jijun and others developed a method to process external beveloid gears in 2014 based on the gear processing principle of a gear hobbing machine [8]. Wu Junfei and others proposed a method to process the internal beveloid gears using a gear shaper in 2000, which offered a more trustworthy approach for the actual processing research of the internal beveloid gear [9]. Chen suggests processing internal beveloid gear using a gear shaper under multiple degrees of freedom [10]. A beveloid non−circular gear transmission scheme was developed by J Han to improve stability and accuracy, reducing meshing impact and allowing backlash adjustment [11]. An adaptive design model is proposed by Bing Cao et al. for the continuous generation of beveloid gears in common gear grinding machines [12].

A gear dynamics model that takes into account mass and equivalent spring force was developed based on Tuplin's initial hypothesis that, under certain assumptions, a pair of

meshing gears can be substituted by an elastic nonlinear model. This hypothesis was first put forth in 1950 [13,14]. With the advancement of computers, numerical techniques can be utilized to examine the nonlinearity of gear teeth. The Runge–Kutta method is the most popular of them. Wang Xiaosun analyzes the nonlinear properties of the transmission through Poincaré sections, bifurcation diagrams, power spectra, etc. using the variable step size Gill technique [15]. A higher damping coefficient and the proper backlash can suppress the chaotic region, according to analysis by Gao et al. using the Runge–Kutta numerical integration method [16]. The six degree of freedom gear's vibration analysis model was numerically studied by Jiang H et al. The findings demonstrate that when the gear teeth's peeling area increases, the dynamic response's oscillation at its beginning and end becomes more important [17]. Yang et al. created a gear tooth torsional vibration analysis model taking into account variables like multiple harmonic excitations [18]. Robert G. examined the planetary gear's nonlinear dynamics using numerical and analytical techniques in 2010, and he evaluated the precision of the calculations using finite elements and numerical integrated simulation [19]. G Yu et al. examined the contact behavior between the meshing tooth surfaces of curved beveloid gear pairs and a fractal contact mechanics model for the rough surface of a beveloid gear with elliptical asperities was established [20]. A slice−based mesh stiffness modeling method is proposed by Ruihua Sun et al. for straight beveloid gear pair for the calculation of mesh stiffness of irregular tapered tooth profile [21,22].

As demonstrated by the above literature review, the vibration characteristics of internal beveloid gear transmission systems have not been extensively studied, with most research focusing on the machining process of these gears. Additionally, understanding the nonlinear behavior of gear systems is crucial for accurately predicting their performance and optimizing their design, but there is a dearth of research on the nonlinear properties of gear systems, particularly when considering multiple degrees of freedom and parameter coupling. Therefore, this paper investigates the nonlinear vibration characteristics of internal beveloid gears under various external and internal factors. It explores the influence of these factors on the gear system's vibration behavior, aiming to optimize its design and reduce vibration and noise levels.

2. Dynamic Model of Internal Beveloid Gear System

Table 1 displays the geometric specifications of the internal beveloid gear transmission system.

Table 1. Geometric parameters of internal beveloid gear transmission system.

Gear Parameters	External Gear	Internal Gear
Number of teeth	$Z_1 = 45$	$Z_2 = 60$
Module	$m = 2.5$	$m = 2.5$
Pressure angle of rack cutter/°	$\alpha = 20$	$\alpha = 20$
Machining pitch angle/°	$\delta = 5$	$\delta = 5$
Coefficient of addendum h_a^*	0.55	0.55
Coefficient of bottom clearance h_i^*	0.25	0.25
Face width/mm	$b_1 = 22.5$	$b_2 = 22.5$
Mass/kg	1.345	1.312
Moment of inertia/kg · m^2	0.002550	0.009016

From the large end of the beveloid gear, the dividing circle pressure angle on the end face and dividing circle helix angle can be expressed as:

$$\alpha_{\mathrm{tL(R)}} = \arctan\left(\frac{\tan\alpha_{\mathrm{n}}\cos\delta}{\cos\beta'} \pm \sin\delta\tan\beta'\right) \tag{1}$$

$$\beta_{\mathrm{R(L)}} = \arctan\left(\cos\delta\tan\beta' \mp \frac{\tan\alpha_{\mathrm{n}}\sin\delta}{\cos\beta'}\right) \tag{2}$$

where δ is the machining pitch angle of beveloid gear (rad), β' is the cutting tool helix angle (rad), and α_n is the dividing circle normal pressure angle (rad).

For parallel−axis beveloid gears, both gears are manufactured using straight−tooth racks. The dividing circle pressure angle and the dividing circle helix angle on the end face can be expressed as:

$$\alpha_{tL1} = \alpha_{tR2} = \arctan(\tan\alpha_n \cos\delta) \tag{3}$$

$$\beta_{L1} = \beta_{R2} = \arctan(\tan\alpha_n \sin\delta) \tag{4}$$

In order to assist the study, the dynamic model is constructed with a number of fundamental assumptions. It is assumed that both gears are ideal rigid bodies and that the meshing force of the gears is equal to the spring−damper model in the direction of the path of contact; it is assumed that the installation position of the two gears is ideal and unchanged, and there are no influencing factors such as tooth eccentricity, regardless of the impact between the tooth meshing and the influence of the gear meshing and bearing−related friction factors. Therefore, the internal beveloid gear's bend−torsion−bend 3−DOF vibration model is established. The model is represented by Figure 1.

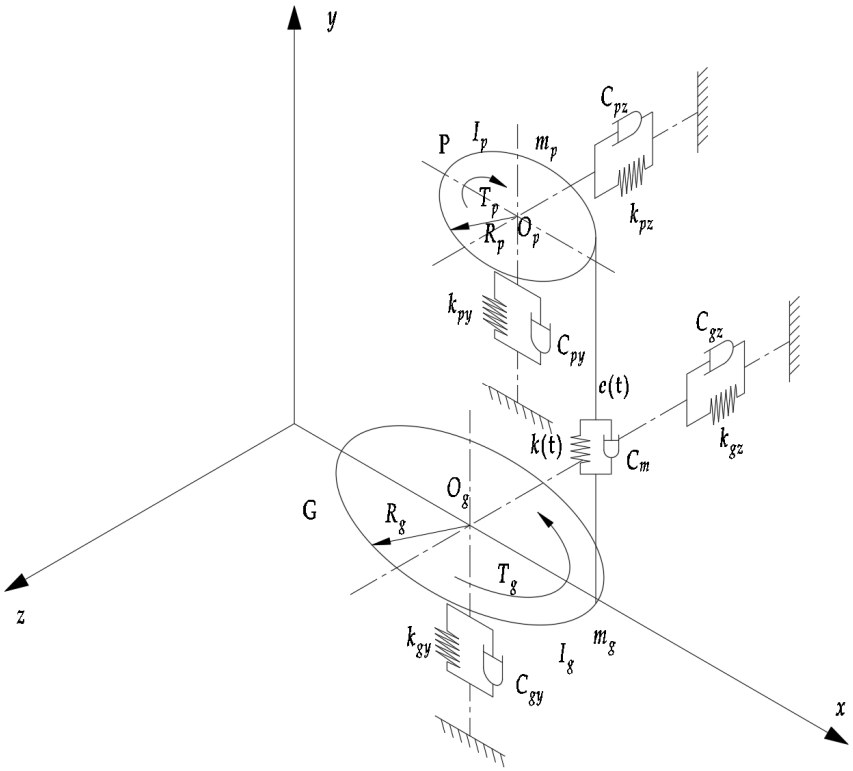


Figure 1. Dynamic model of internal beveloid gear.

The internal beveloid gear transmission's variable coordinate X is

$$X = [y_p, z_p, \theta_p, y_g, z_g, \theta_g] \tag{5}$$

where $y_i, z_i, \theta_i (i = p, g)$ are the relative vibration displacement and angular vibration angular displacement of the center of mass of the pinion and gear in the y and z axes, respectively.

At the point where two gears mesh, the connection between their radial and axial vibration displacements may be represented as:

$$\overline{z} = \overline{y} \tan\beta_p \tag{6}$$

The expression for the radial and axial vibrational displacement offset at the meshing point of the external gear is:

$$\overline{y}_1 = \overline{y}_p + \overline{\theta}_p R_p \tag{7}$$

$$\overline{z}_1 = \overline{z}_p - \left(\overline{y}_p + \overline{\theta}_p R_p\right) \tan\beta_p \tag{8}$$

The expression for the radial and axial vibrational displacement offset at the meshing point of the ring gear is:

$$\overline{y}_2 = \overline{y}_g - \overline{\theta}_g R_g \tag{9}$$

$$\overline{z}_2 = \overline{z}_g - \left(\overline{y}_g - \overline{\theta}_g R_g\right) \tan\beta_p \tag{10}$$

The gear transmission system's properties can be described as meshing stiffness k_m, meshing damping c_m, transmission error e, and normal tooth backlash 2 b on the $y-$ and $z-$axes, respectively:

$$\begin{cases} k_{\mathrm{m}y} = k_{\mathrm{m}} \cos\beta_p & k_{\mathrm{m}z} = k_{\mathrm{m}} \sin\beta_p \\ c_{\mathrm{m}y} = c_{\mathrm{m}} \cos\beta_p & c_{\mathrm{m}z} = c_{\mathrm{m}} \sin\beta_p \\ e_y = e\cos\beta_p & e_z = e\sin\beta_p \\ b_y = b\cos\beta_p & b_z = b\sin\beta_p \end{cases} \tag{11}$$

The radial meshing component of the gear is

$$\begin{aligned} F_y &= k_{my}(\overline{t})\overline{f}_y\left(\overline{y}_1 - \overline{y}_2 - \overline{e}_y\right) + c_{my}\left(\dot{\overline{y}}_1 - \dot{\overline{y}}_2 - \dot{\overline{e}}_y\right) \\ &= \cos\beta_p\left[k_m\overline{f}_y\left(\overline{y}_p + \overline{\theta}_p R_p - \overline{y}_g + \overline{\theta}_g R_g - \overline{e}_y\right)\right. \\ &\left. + c_{\mathrm{m}}\left(\dot{\overline{y}}_p + \dot{\overline{\theta}}_p R_p - \dot{\overline{y}}_g + \dot{\overline{\theta}}_g R_g - \dot{\overline{e}}_y\right)\right] \end{aligned} \tag{12}$$

The change in the modification coefficient of the beveloid gear creates a slight bevel angle along the axis, generating an axial force along the small end of the gear toward the large end. To the pinion:

$$F_{\mathrm{a}} = \frac{2\,\overline{T}_{pm}}{\mathrm{d}_p} \frac{\tan\alpha_{\mathrm{n}}}{\cos\beta} \sin\delta \tag{13}$$

where d_p is the dividing circle diameter of pinion (m) and β is helical angle of the dividing circle (rad). Considering the bevel angular component, the meshing component of the axial is:

$$\begin{aligned} F_z' &= F_{\mathrm{z}} \pm F_{\mathrm{a}} = k_{mz}(\overline{t})\overline{f}_z(\overline{z}_1 - \overline{z}_2 - \overline{e}_z) + c_{mz}\left(\dot{\overline{z}}_1 - \dot{\overline{z}}_2 - \dot{\overline{e}}_z\right) \pm F_{\mathrm{a}} \\ &= \sin\beta_p\left\{k_{\mathrm{m}}\overline{f}_z\left[\overline{z}_p - \left(\overline{y}_p + \overline{\theta}_p R_p\right)\tan\beta_p - \overline{z}_g + \left(\overline{y}_g - \overline{\theta}_g R_g\right)\tan\beta_p - \overline{e}_z\right]\right. \\ &\left. + c_{\mathrm{m}}\left[\dot{\overline{z}}_p - \left(\dot{\overline{y}}_p + \dot{\overline{\theta}}_p R_p\right)\tan\beta_p - \dot{\overline{z}}_g + \left(\dot{\overline{y}}_g - \dot{\overline{\theta}}_g R_g\right)\tan\beta_p - \dot{\overline{e}}_z\right]\right\} \pm F_{\mathrm{a}} \end{aligned} \tag{14}$$

On the basis of Newton's law, a dynamic equivalent model of the internal beveloid gear is developed:

$$m_p\ddot{\overline{y}}_p + c_{py}\dot{\overline{y}}_p + k_{py}\overline{f}_b\left(\overline{y}_p\right) = -F_y \tag{15}$$

$$m_p\ddot{\overline{z}}_p + c_{pz}\dot{\overline{z}}_p + k_{pz}\overline{f}_b\left(\overline{z}_p\right) = F_z + F_a \tag{16}$$

$$I_p\ddot{\theta}_p = \overline{T}_p - F_y R_p \tag{17}$$

$$m_g\ddot{\overline{y}}_g + c_{g\mathrm{y}}\dot{\overline{y}}_g + k_{\mathrm{g}y}\overline{f}_b\left(\overline{y}_g\right) = -F_y \tag{18}$$

$$m_g\ddot{\bar{z}}_g + c_{gz}\dot{\bar{z}}_g + k_{gz}\bar{z}_b(\bar{z}_g) = -F_z - F_a \tag{19}$$

$$I_g\ddot{\bar{\theta}}_g = -\overline{T}_g + F_y R_g \tag{20}$$

According to Formulas (15)–(20), the gear transmission system's differential equations may be derived. Each gear has three generalized degrees of freedom and each degree of freedom has a vibration differential equation.

$$\begin{aligned} &m_p\ddot{\bar{y}}_p + c_m\left(\dot{\bar{y}}_p - \dot{\bar{y}}_g + R_p\dot{\bar{\theta}}_p + R_g\dot{\bar{\theta}}_g - \dot{\bar{e}}_y\right)\cos\beta_p + k_{py}\overline{f}_b\left(\bar{y}_p\right) \\ &+c_{py}\dot{\bar{y}}_p + k_m(\bar{t})f_y\left(\bar{y}_p - \bar{y}_g + R_p\bar{\theta}_p + R_g\bar{\theta}_g - \bar{e}_y\right)\cos\beta_p = 0 \end{aligned} \tag{21}$$

$$\begin{aligned} &m_p\ddot{\bar{z}}_p - c_m\left[\dot{\bar{z}}_\mathrm{p} - \dot{\bar{z}}_\mathrm{g} - \left(\dot{\bar{y}}_p - \dot{\bar{y}}_g + R_p\dot{\bar{\theta}}_p + R_g\dot{\bar{\theta}}_g - \dot{\bar{e}}_y\right)\tan\beta_p\right]\sin\beta_p + k_{pz}\overline{f}_b(\bar{z}_p) \\ &+c_{pz}\dot{\bar{z}}_p - k_m(\bar{t})f_z\left[\bar{z}_\mathrm{p} - \bar{z}_\mathrm{g} - \left(\bar{y}_p - \bar{y}_g + R_p\bar{\theta}_p + R_g\bar{\theta}_g - \bar{e}_y\right)\tan\beta_p\right]\sin\beta_p = F_a \end{aligned} \tag{22}$$

$$\begin{aligned} &I_p\ddot{\bar{\theta}}_p + R_p c_m\left(\dot{\bar{y}}_p - \dot{\bar{y}}_g + R_p\dot{\bar{\theta}}_p + R_g\dot{\bar{\theta}}_g - \dot{\bar{e}}_y\right)\cos\beta_p \\ &+R_p k_m(\bar{t})f_y\left(\bar{y}_p - \bar{y}_g + R_p\bar{\theta}_p + R_g\bar{\theta}_g - \bar{e}_y\right)\cos\beta_p = \overline{T}_p \end{aligned} \tag{23}$$

$$\begin{aligned} &m_g\ddot{\bar{y}}_g - c_m\left(\dot{\bar{y}}_p - \dot{\bar{y}}_g + R_p\dot{\bar{\theta}}_p + R_g\dot{\bar{\theta}}_g - \dot{\bar{e}}_y\right)\cos\beta_p + k_{gy}\overline{f}_b\left(\bar{y}_g\right) \\ &+c_{gy}\dot{\bar{y}}_g - k_m(\bar{t})f_y\left(\bar{y}_p - \bar{y}_g + R_p\bar{\theta}_p + R_g\bar{\theta}_g - \bar{e}_y\right)\cos\beta_p = 0 \end{aligned} \tag{24}$$

$$\begin{aligned} &m_g\ddot{\bar{z}}_g + c_m\left[\dot{\bar{z}}_\mathrm{p} - \dot{\bar{z}}_\mathrm{g} - \left(\dot{\bar{y}}_p - \dot{\bar{y}}_g + R_p\dot{\bar{\theta}}_p + R_g\dot{\bar{\theta}}_g - \dot{\bar{e}}_y\right)\tan\beta_p\right]\sin\beta_p + k_{gz}\overline{f}_b(\bar{z}_g) \\ &+c_{gz}\dot{\bar{z}}_g + k_m(\bar{t})f_z\left[\bar{z}_\mathrm{p} - \bar{z}_\mathrm{g} - \left(\bar{y}_p - \bar{y}_g + R_p\bar{\theta}_p + R_g\bar{\theta}_g - \bar{e}_y\right)\tan\beta_p\right]\sin\beta_p = -F_a \end{aligned} \tag{25}$$

$$\begin{aligned} &I_g\ddot{\bar{\theta}}_g - R_g c_m\left(\dot{\bar{y}}_p - \dot{\bar{y}}_g + R_p\dot{\bar{\theta}}_p + R_g\dot{\bar{\theta}}_g - \dot{\bar{e}}_y\right)\cos\beta_p \\ &-R_g k_m(\bar{t})f_z\left(\bar{y}_p - \bar{y}_g + R_p\bar{\theta}_p + R_g\bar{\theta}_g - \bar{e}_y\right)\cos\beta_p = -\overline{T}_g \end{aligned} \tag{26}$$

where I_p, I_g are moment of inertia of external and internal gears (kg · m^2); m_p, m_g are mass of external and internal gears (kg); c_p, c_g are bearing support damping of external and internal gears (N · s/m); k_p, k_g are bearing support stiffness of external and internal gears (N/m); $\overline{T}_p$, $\overline{T}_g$ are input and output torque (N · m); $\bar{\theta}_p$, $\bar{\theta}_g$ are relative torsional displacement of external and internal gears (m); $\bar{y}_p$, $\bar{y}_g$ are relative radial displacement of external and internal gears (m); $\bar{z}_p$, $\bar{z}_g$ are relative axial displacement of external and internal gears (m).

Table 2 shows the calculated values of bearing support stiffness and damping.

Table 2. Calculation of bearing support stiffness and damping.

Bearing Support Stiffness		**Bearing Support Damping**	
Bearing Radial Support Stiffness k_y (N/m)	**Bearing Axial Support Stiffness k_z (N/m)**	**Bearing Radial Support Damping $c_y$dsad (N·s/m)**	**Bearing Axial Support Damping c_z(N·s/m)**
1.364×10^8	7.173×10^7	2708	1964

Table 3 displays additional gear transmission system parameters.

Table 3. Additional gear transmission system parameters.

Meshing Damping	Backlash	
	Tooth Backlash	**Bearing Backlash**
2595.6 N · s/m	$f(x) = \begin{cases} x-b & (x>b) \\ 0 & (-b \le x \le b) \\ x+b & (x<-b) \end{cases}$	$\overline{f}_b(\overline{x}) = \begin{cases} \overline{x}-b_b & (\overline{x}>b_b) \\ 0 & (-b_b \le x \le b_b) \\ \overline{x}+b_b & (x<-b_b) \end{cases}$
	Error stimulation	Excitation
	$e(t) = e_r \sin \omega_n t$	$T(t) = T_{at} + T_f \sin(\omega t)$

Note: In order to facilitate the calculation, the seventh−order fitting can be used, and the fitting function is $f(x,b) = \sum_{n=1}^{7} a_{2n-1}x^{2n-1} = a_1x + a_2x^2 + a_3x^3 + a_4x^4 + a_5x^5 + a_6x^6 + a_7x^7$. e_r—Gear error amplitude. In this paper, 20 μm is taken. ω_n —Gear pair meshing angular frequency. T_f —First order amplitude of torque fluctuation (N · m), valued at 5% of theoretical torque. ω —First order harmonic angular frequency.

3. Numerical Solution of Internal Beveloid Gear with Parallel Axes

When studying gear meshing, it is common to equivalently represent the meshing portion as a spring−damper connection. Essentially, solving the dynamic model of a gear transmission system involves transforming the gear dynamics model into a system of multivariate differential equations that consider time−varying meshing stiffness, meshing damping, tooth backlash, and other parameters. The Runge–Kutta method is widely applied in numerical solutions.

In this study, the Runge–Kutta method was chosen to solve the system of multivariate differential equations due to its advantages of high accuracy, stability, flexibility, scalability, and ease of implementation. The Runge–Kutta method effectively approximates the solutions of differential equations, and by adjusting the step size and order, it allows for a balance between computational accuracy and efficiency. Furthermore, this method exhibits good applicability to nonlinear and stiff equations. By adopting the Runge–Kutta method, we can obtain more accurate numerical solutions for the system of multivariate differential equations, providing robust support for modeling and analysis in practical problems.

3.1. Analysis of Nonlinear Vibration Characteristics

When solving by the Runge–Kutta method, it is necessary to first reduce the original 6 s−order ordinary differential equations to 12 first−order ordinary differential equations. This section investigates the impact of factors on the nonlinear vibration characteristics of the transmission system under the action of multi−excitation coupling and discusses the effects of torque fluctuation and bearing clearance on the vibration characteristics. Take the rotational speed $n = 1000$ r/min, excitation $T_{at} = 10$ N · m, torque fluctuation $T_f = 0.05\ T_{at}$N · m, transmission error $E = 20$ μm, tooth backlash $2\ b = 10$ μm, and bearing backlash $b_b = 20$ μm. The time domain and frequency domain responses of radial and axial vibration displacement of a gear pair are derived.

Under the above parameters, the nonlinear vibration characteristics of the internal beveloid gear pair are analyzed.

Taking into account the non−steady state response in the early phase of the vibration response, this paper solves the system response in the period 0~3 s, and uses the vibration−displacement response curve of the steady−state response period 2.95 s~3.00 s to solve the radial and axial vibration−displacement response curve of each gear and frequency domain response curve. As shown in Figure 2 below.

On the basis of the vibration−displacement response curves of Figure 2a–d, it is evident that the relative displacement responses of the radial and axial directions of the gears correspond to each other, therefore the ensuing analysis only concerns the external gear. The radial vibration displacement of the external gear has an amplitude of 30.975 μm, whereas the axial vibration displacement has an amplitude of 6.8650 μm. It can be shown that, under these conditions, the axial vibration displacement has minimal effect on the transmission system's vibration amplitude, and its radial vibration is the dominating one.

At the same time, it is discovered that the radial and axial vibration responses oscillate based on the new steady−state equilibrium point after a certain offset. Although its axial vibration amplitude is tiny, its offset from the equilibrium point is not significantly different from the radial vibration offset. The subsequent study will reveal that the offset value of the equilibrium point of the vibration response has a significant link with the bearing backlash.

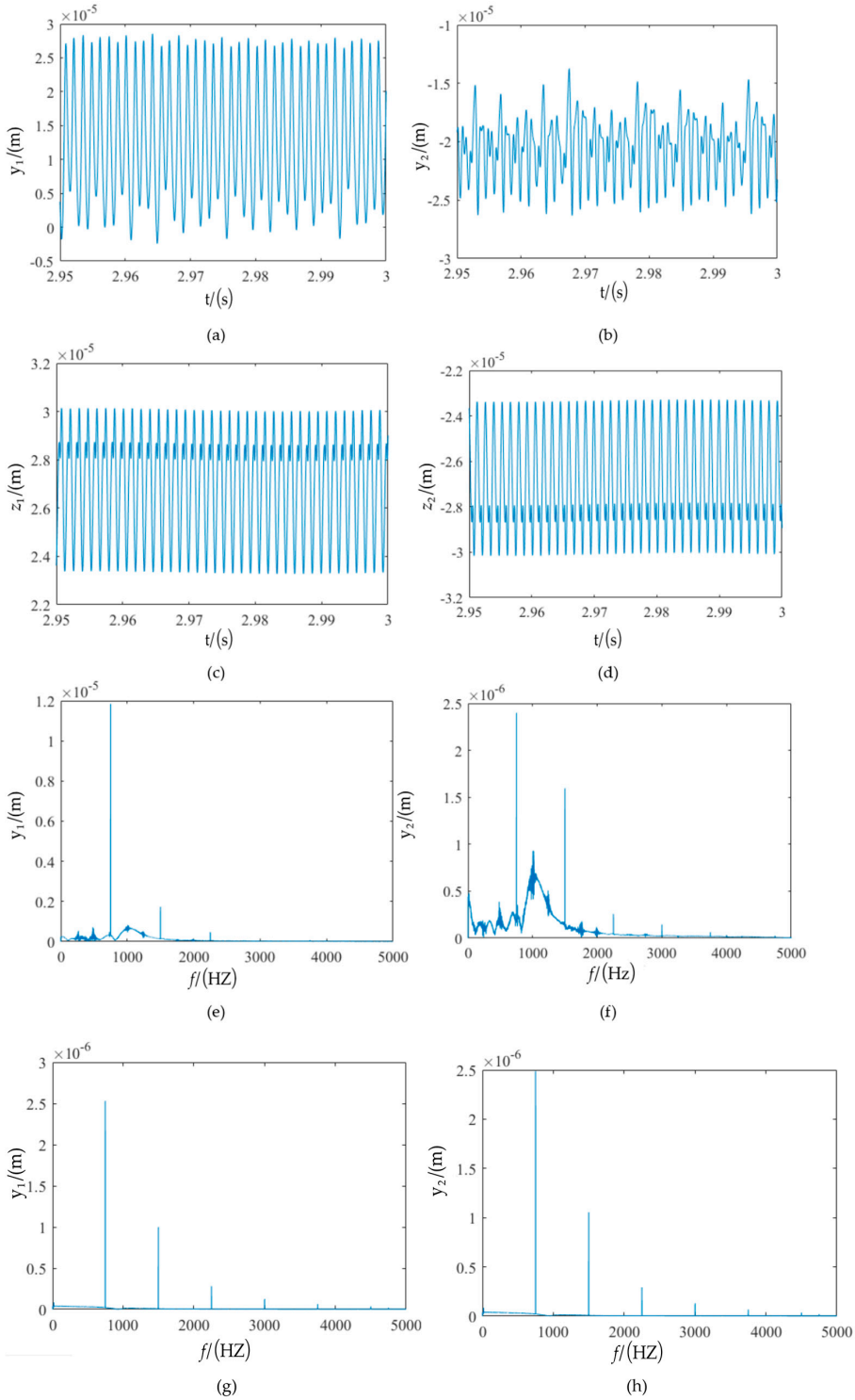


Figure 2. Gear vibration−displacement response curve and spectrogram (**a**,**b**) the radial time domain response of external gear and internal gear; (**c**,**d**) the axial time domain response of external gear and internal gear; (**e**,**f**) the radial spectrogram of external gear and internal gear; (**g**,**h**) the axial spectrogram of external gear and internal gear.

Figure 2e–h show that when the rotational speed is n = 1000 r/min, the gear rotating frequency is n/60 Hz, so the meshing frequency is nz/60 = 750 Hz. According to the spectrogram, it can be observed that the peaks of the radial vibration and axial vibration of the gear are at the meshing frequency, and the subsequent peaks are essentially n times the meshing frequency, which is consistent with the theoretical situation. The harmonic properties of the gear's radial vibration are highly pronounced, with a multitude of small peaks. At 2 kHz, the vibration amplitude swings significantly, the vibration is intense, and the level of nonlinearity is considerable. In the axial position, it also has noticeable multiple peaks, and the corresponding frequency value is an integer multiple of the meshing frequency, but nearly no small peaks and its periodic vibration is rather steady.

3.2. Influence of Excitation Parameters on Nonlinear Vibration Characteristics of Transmission System

3.2.1. Effect of Bearing Backlash on Vibration

Both the bearing backlash parameters and tooth backlash parameters are piecewise functions. This work does not differentiate between radial and axial bearing backlash when analyzing the bearing backlash function; both are assigned the same value. Considered is the vibration response when the bearing backlash $b_b = 20$ μm, and bearing backlash $b_b = 0$ μm, input speed $n = 1000$ r/min, excitation $T_{at} = 10$ N · m, torque fluctuation $T_f = 0.05\ T_{at}$N · m, transmission error $E = 20$ μm, tooth backlash 2 $b = 10$ μm, the vibration−displacement response and frequency domain response curves are obtained for the external gear. As seen in Figure 3 below.

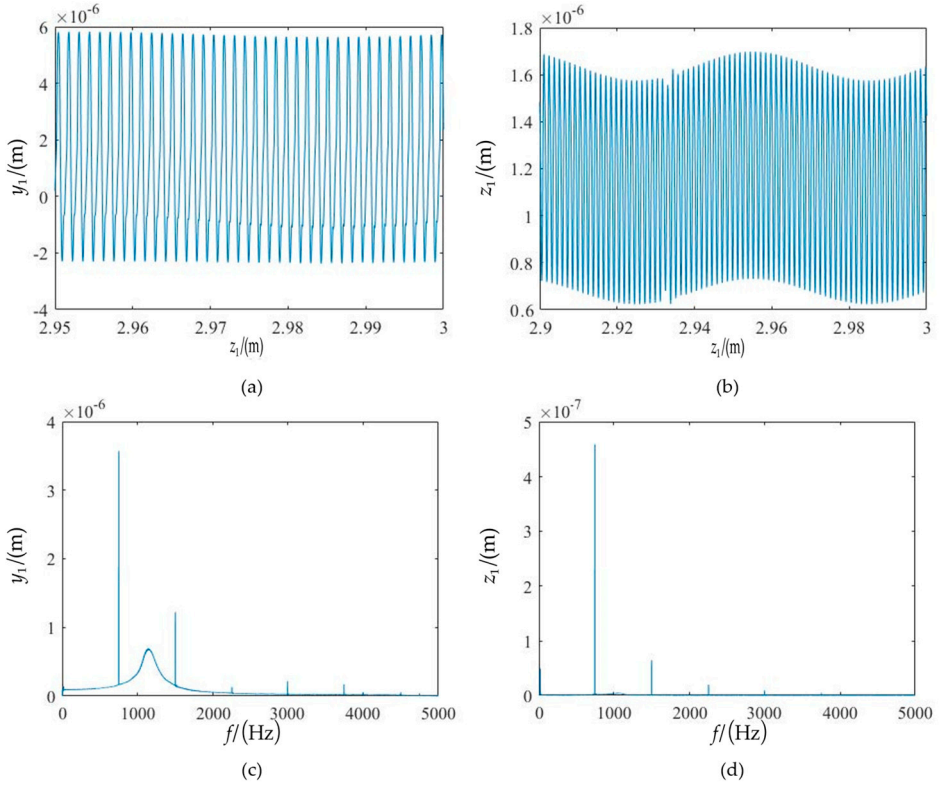


Figure 3. Time domain response and spectrogram of vibration displacement with bearing backlash $b_b = 0$ μm (**a**,**b**) the radial and axial time responses of external gear; (**c**,**d**) the radial and axial spectrograms of external gear.

Comparing Figure 2a,e and Figure 3a,c, it can be observed that when the bearing backlash $b_b = 0$ μm is used, the radial time domain response of the gear exhibits improved periodicity, and the harmonic characteristics of the frequency domain response are weakened. The nonlinear vibration characteristics are also weakened, and the harmonic characteristics of the frequency at which the peak value is located do not change. Evidently,

the bearing backlash has a significant impact on the degree of radial nonlinear vibration of the gear and enhances the nonlinear vibration of the gear pair.

Comparing Figure 2c,f and Figure 3b,e, it is evident that when the impact of bearing backlash is disregarded, the axial vibration periodicity is more pronounced, the frequency domain response harmonic characteristics vary less, and the vibration amplitude varies significantly. It can also be observed that the axial displacement equilibrium point varies with the harmonic function. When analyzing the effect of excitation, it will be indicated later that the mean change is connected to the excitation torque fluctuations T_f.

3.2.2. Influence of Torque Fluctuation on Vibration

As shown in Figure 3b, the mean value of its axial vibration varies with time according to a simple harmonic function. This phenomenon is connected to the variation in the input torque, as determined by its fluctuation frequency and axial vibration equation.

Ignore the bearing backlash, use the torque fluctuation $T_f = 0, 0.05$ and $0.2\ T_{at}\mathrm{N} \cdot \mathrm{m}$, and generate the vibration time domain curve comparison diagram as depicted in Figures 4 and 5 below.

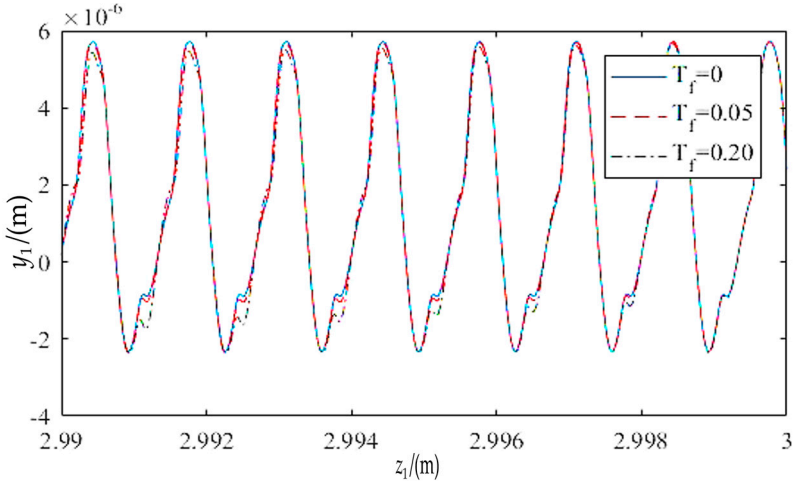


Figure 4. Time domain diagram of external gear radial vibration under different torque fluctuations.

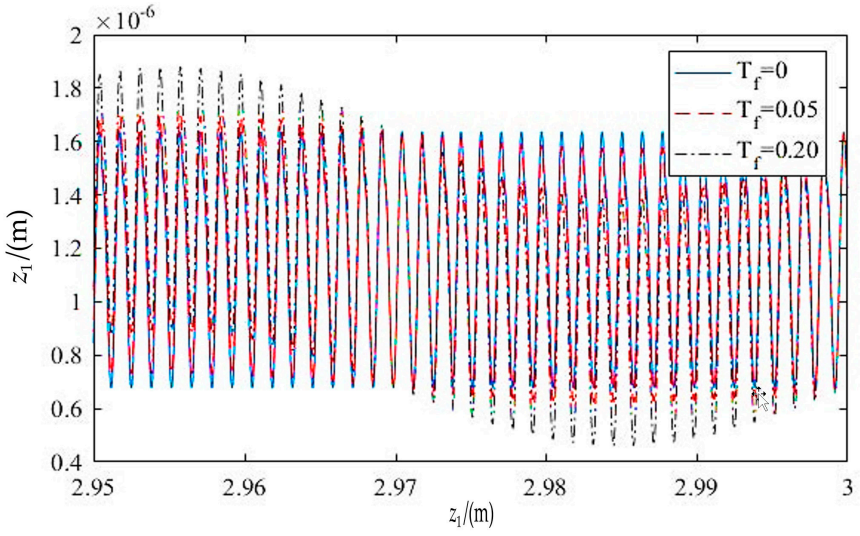


Figure 5. Time domain diagram of external gear axial vibration under different torque fluctuations.

Figures 4 and 5 show that the radial vibration amplitude is 8.053 µm, 8.111 µm, and 8.475 µm when the torque fluctuation is $T_f = 0, 0.05, 0.2\ T_{at}\mathrm{N} \cdot \mathrm{m}$, whereas the axial

vibration amplitude is 0.960 μm, 1.064 μm, and 1.419 μm. The presence of torque fluctuation causes the change in the gear's axial vibration equilibrium point to appear as a near−harmonic vibration with the torque fluctuation, hence increasing its axial vibration amplitude. Under these conditions, the effect of torque fluctuation on the radial vibration of the gear is not readily apparent. With a rise in torque fluctuation, the vibration peak rises little, whereas the vibration trend rarely alters. In light of the fact that the input torque selected at this moment is minimal, the change in its radial and axial vibration amplitude is not readily apparent. When the input torque rises, the torque fluctuation's degree of effect will grow.

In order to better assess the influence of parameter changes on the vibration of gears at all levels, further study disregards the influence of torque fluctuation for the time being and uses $T_f = 0$ N · m.

3.2.3. Influence of Input Torque on Vibration

The influence of torque fluctuation has been analyzed above, torque fluctuation $T_f = 0$ N · m, input speed $n = 1000$ r/min, bearing backlash $b_b = 20$ μm, transmission error $E = 20$ μm, tooth backlash $2\,b = 10$ μm, and change the input torque $T_{at} = 10,\ 15,\ 20$ N · m to obtain the time domain graph of external gear vibration, as shown in Figures 6 and 7 below.

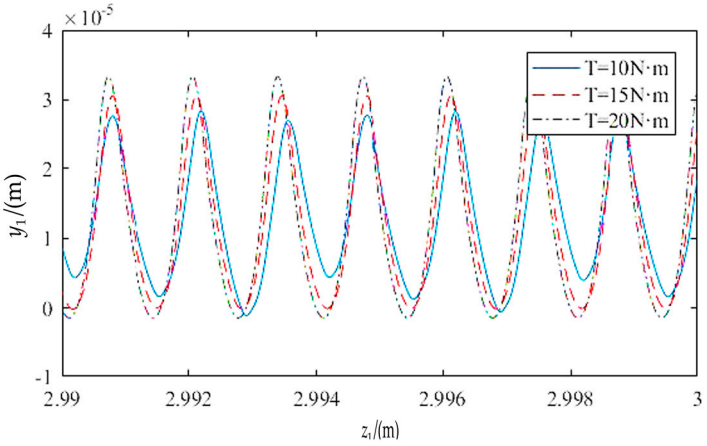


Figure 6. Time domain diagram of external gear radial vibration under different input torques.

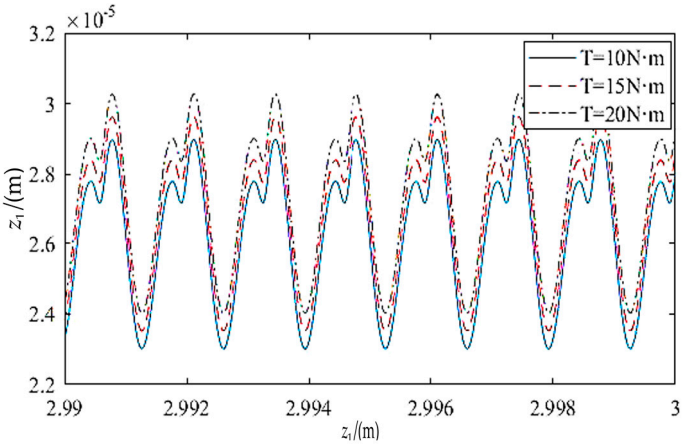


Figure 7. Time domain diagram of external gear axial vibration under different input torques.

In accordance with Figures 6 and 7, when the input torque is $T_{at} = 10,\ 15,\ 20$ N · m the radial vibration amplitude is 29.738 μm, 30.938 μm, and 34.828 μm, while the axial vibration amplitude is 6.754 μm, 6.875 μm, and 7.019 μm.

When the torque increases from 10 N · m to 20 N · m, the external gear's radial vibration peaks and troughs increase simultaneously, as does the amplitude, yet the equilibrium point hardly shifts. The equilibrium point of the axial vibration curve of the external gear displays a clear rising tendency overall. Simultaneously, the amplitude grows but the changing trend of the two curves remains unchanged.

3.2.4. Influence of Tooth Backlash on Vibration

In the process of producing gears, flaws such as base bitch and gear tooth profile are unavoidable. To decrease friction heat and improve transmission performance, a particular lubrication backlash must be left. Moreover, the presence of tooth backlash affects the transmission accuracy of the gear, resulting in impact and noise, which has a significant influence on the vibration characteristics of the gear pair.

When the input speed $n = 1000$ r/min, the excitation $T_{at} = 10$ N · m, the transmission error $E = 20$ μm, the torque fluctuation is $T_f = 0$ N · m, and the bearing backlash $b_b = 20$ μm, the backlash's general value range is considered. Take the tooth backlash 2 $b = 0, 10, 100$ μm to produce the time−domain curve comparison diagram of the external gear vibration, as well as the radial comparison Figure 8 and the axial comparison Figure 9.

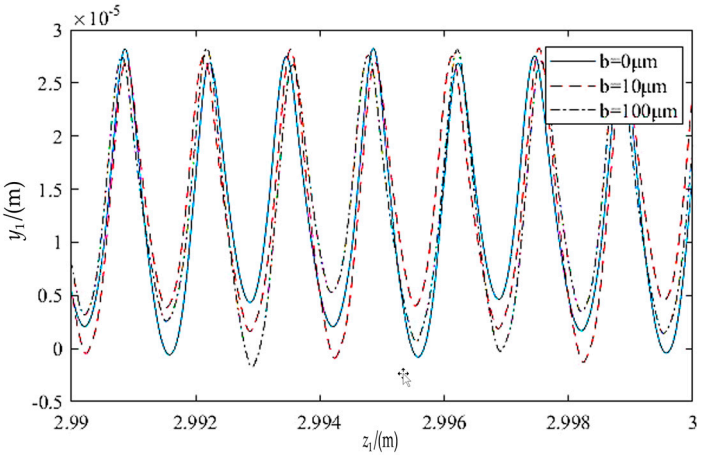


Figure 8. Time domain diagram of radial vibration of external gear under different tooth backlashes.

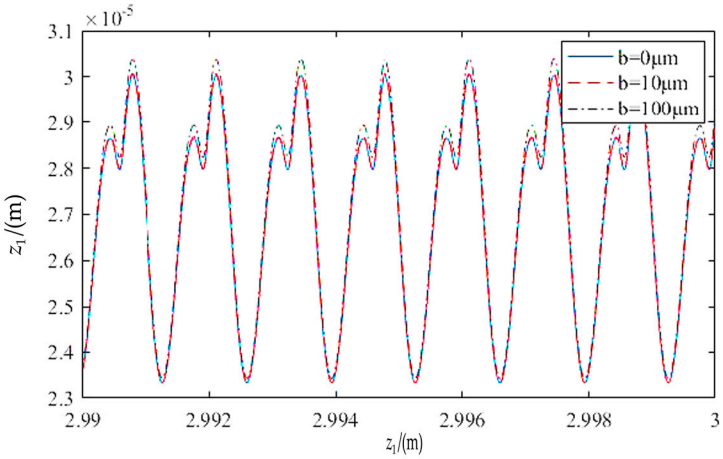


Figure 9. Time domain diagram of axial vibration of external gear under different tooth backlashes.

When the tooth backlash 2 $b = 0, 10, 100$ μm, the radial vibration amplitude is 29.208 μm, 29.738 μm, and 30.698 μm, respectively, and the axial vibration amplitude is 6.706 μm, 6.754 μm, and 6.981 μm, respectively. When the backlash changes, the radial vibration curve of the gear changes under the coupling action of bearing backlash, but it is difficult to

analyze. The vibration amplitude increases to a certain degree, the axial vibration trough rises little, and the peak value rises significantly. The global amplitude increases.

3.2.5. Influence of Input Speed on Vibration

In accordance with the meshing angular frequency formula, the input speed of the transmission system directly defines its meshing angular frequency, while the meshing angular frequency specifies the period of error excitation and the vibration response will peak at this frequency.

Excitation $T_{at} = 10\,\mathrm{N \cdot m}$, transmission error $E = 20\,\mu\mathrm{m}$, torque fluctuation is $T_f = 0\,\mathrm{N \cdot m}$, bearing backlash $b_b = 0\,\mu\mathrm{m}$, tooth backlash $2\,b = 10\,\mu\mathrm{m}$, and input speed n = 900, 1000, 1100 r/min respectively, to obtain the time domain curve comparison diagram of external gear vibration, as shown in Figures 10 and 11.

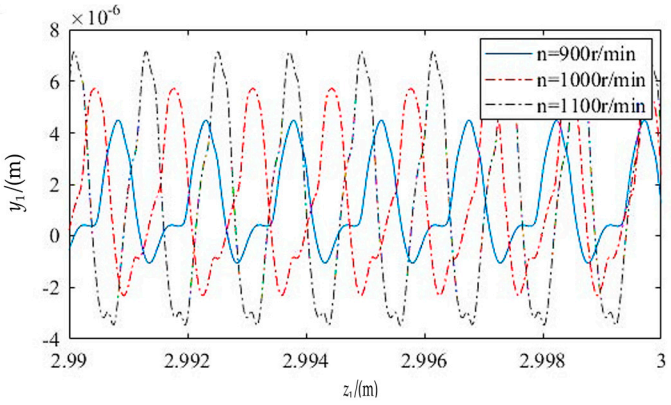


Figure 10. Time domain diagram of radial vibration of external gear at different rotational speeds.

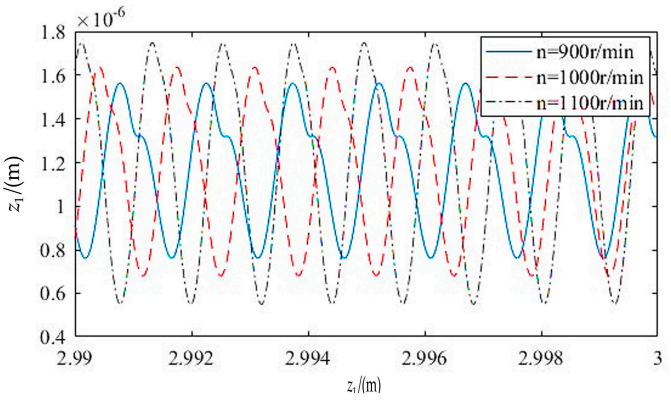


Figure 11. Time domain diagram of axial vibration of external gear at different rotational speeds.

Figures 10 and 11 indicate that for n = 900, 1000, 1100 r/min, the radial vibration amplitude is 5.578 μm, 8.059 μm, and 10.729 μm, whereas the axial vibration amplitude is 0.8007 μm, 0.9603 μm, and 1.2034 μm.

Further examination of the radial vibration amplitude of the gear, when the speed is 400 r/min~1200 r/min, reveals that when the input speed is low, the amplitude of the radial and axial vibration curves of the gear pair varies noticeably in the same manner as the speed. When the input speed is between 3000 r/min and 4000 r/min, the vibration amplitude tends to remain steady.

4. Harmonic Balance Analysis

In general, for nonlinear differential equations, exact solutions do not exist unless under very special conditions. Therefore, to obtain analytical results for differential equations,

it is necessary to construct approximate schemes. Nonlinear gear transmission systems have several main theoretical solution methods derived from mathematical deductions, including the harmonic balance method, shooting method, perturbation method, multiscale method, and homotopy analysis method. Among them, the multiscale method and homotopy analysis method have more complex solving processes and present certain challenges in analyzing complex multi−level and multi−parameter coupled transmission systems due to their high computational requirements. On the other hand, the harmonic balance method offers advantages of accuracy, efficiency, controllability, and applicability, making it an effective approach for addressing harmonic vibration problems in differential equation systems. In this chapter, the harmonic balance method is employed for solving and compared with numerical methods. Through frequency response analysis, the influence of rotational speed on the nonlinear transmission system is further examined.

4.1. Solution of Harmonic Balance Method

The harmonic balance method assumes that the variables in the gear transmission system can be approximated as a superposition of multiple harmonics. The approximate harmonic superposition is then substituted into the original parameter equations. By integrating the values corresponding to each harmonic term, a system of equations is obtained to solve for the harmonic coefficients based on the assumed solution. Finally, by substituting the obtained harmonic coefficients into the original variables, an approximate solution for the variables in terms of harmonic superposition can be obtained.

In the majority of instances, the primary determinants of a gear transmission system are its mean value and its first−order harmonic component. Consequently, the solution of the original equation can be represented by the mean value and the first−order harmonic component corresponding to it. Radial, axial, and torsional vibrations of the gear are expressed approximately by their respective first−order harmonic components:

$$y_i = y_i^{\mathrm{s}} \sin(\omega t) + y_i^{\mathrm{c}} \cos(\omega t) \tag{27}$$

$$z_i = z_i^{\mathrm{s}} \sin(\omega t) + z_i^{\mathrm{c}} \cos(\omega t) \tag{28}$$

$$\theta_i = \theta_i^{\mathrm{s}} \sin(\omega t) + \theta_i^{\mathrm{c}} \cos(\omega t) \tag{29}$$

where y_i, z_i, θ_i are radial, axial, and torsional displacements of gear vibration, respectively; y_i^{s}, z_i^{s}, θ_i^{s} are the sinusoidal components of the radial, axial, and torsional displacement of the gear vibration, respectively; y_i^{c}, z_i^{c}, θ_i^{c} are the cosine components of the radial, axial, and torsional displacement of the gear vibration, respectively.

To aid calculation and analysis, the radial, axial, and torsion of the transmission system are written as matrices, and their first− and second−order derivatives are solved:

$$\mathbf{U} = \mathbf{U}^{\mathrm{s}} \sin(\omega t) + \mathbf{U}^{\mathrm{c}} \cos(\omega t) \tag{30}$$

$$\dot{\mathbf{U}} = \omega \mathbf{U}^{\mathrm{s}} \cos(\omega t) - \omega \mathbf{U}^{\mathrm{c}} \sin(\omega t) \tag{31}$$

$$\ddot{\mathbf{U}} = -\omega^2 \mathbf{U}^{\mathrm{s}} \sin(\omega t) - \omega^2 \mathbf{U}^{\mathrm{c}} \cos(\omega t) \tag{32}$$

In the original analysis, the mean value of the gear transmission error is zero, which is described by the harmonic function as:

$$e = e^s \sin(\omega t) \tag{33}$$

where e, e^s are the gear transmission error and the sinusoidal component of the error, respectively.

Simultaneously, the gear transmission error is expressed in matrix form, and its first−order derivative is calculated:

$$\mathbf{E} = \mathbf{E}^{\mathrm{s}} \sin(\omega t) \tag{34}$$

$$\dot{\mathbf{E}} = \omega \mathbf{E}^{\mathrm{s}} \cos(\omega t) \tag{35}$$

Substitute Equations (27)–(35) into differential Equations (23)–(26) of single−stage internal gear vibration, obtain 6 equations, and organize them into matrix form:

$$\begin{array}{c} -\omega^2 \mathbf{M}\mathbf{U}^{\mathrm{s}} \sin(\omega t) - \omega^2 \mathbf{M}\mathbf{U}^{\mathrm{c}} \cos(\omega t) + \omega \mathbf{C}\mathbf{U}^{\mathrm{s}} \cos(\omega t) \\ -\omega \mathbf{C}\mathbf{U}^{\mathrm{c}} \sin(\omega t) + \mathbf{K} f(\mathbf{U}, b) + \mathbf{K}'' f_b(\mathbf{U}'', bb) = 0 \end{array} \tag{36}$$

where $f(\mathbf{U},\ b)$, $f_b(\mathbf{U}'',\ bb)$ represent bearing backlash and tooth backlash functions, respectively.

In order to assist calculation, the tooth backlash function is stated as a first−order polynomial, the radial and axial backlash coefficients are a and b, respectively, and the meshing stiffness is chosen as the average stiffness. The matrix form is represented as follows:

$$\begin{array}{l} -\omega^2 \mathbf{M}\mathbf{U}^{\mathrm{s}} \sin(\omega t) - \omega^2 \mathbf{M}\mathbf{U}^{\mathrm{c}} \cos(\omega t) + \omega \mathbf{C}\mathbf{U}^{\mathrm{s}} \cos(\omega t) - \omega \mathbf{C}\mathbf{U}^{\mathrm{c}} \sin(\omega t) + \mathbf{K}''\mathbf{U} \\ +\mathbf{K}\mathbf{U}^{\mathrm{s}} \sin(\omega t) + \mathbf{K}\mathbf{U}^{\mathrm{c}} \cos(\omega t) = \omega \mathbf{C}'\mathbf{E}^{\mathrm{s}} \cos(\omega t) + \mathbf{K}'\mathbf{E}^{\mathrm{m}} + \mathbf{K}'\mathbf{E}^{\mathrm{s}} \sin(\omega t) \end{array} \tag{37}$$

According to the principle of the harmonic balance approach, the coefficients of the same harmonic term of the matrix equation are set to zero, resulting in a nonlinear differential equation with six equations matching the sine and cosine terms. The matrix is represented as follows:

$$\begin{cases} -\omega^2 \mathbf{M}\mathbf{U}^{\mathrm{s}} - \omega \mathbf{C}\mathbf{U}^{\mathrm{c}} + \mathbf{K}''\mathbf{U}^{\mathrm{s}} + \mathbf{K} f(\mathbf{U}^{\mathrm{s}}, b) = \mathbf{K}'\mathbf{E}^{\mathrm{s}} \\ -\omega^2 \mathbf{M}\mathbf{U}^{\mathrm{c}} + \omega \mathbf{C}\mathbf{U}^{\mathrm{s}} + \mathbf{K}''\mathbf{U}^{c} + \mathbf{K} f(\mathbf{U}^{\mathrm{c}}, b) = \omega \mathbf{C}'\mathbf{E}^{\mathrm{s}} \end{cases} \tag{38}$$

The backlash function is identical to the algebras a, b for combining the $\mathbf{K}''$ term with the original $\mathbf{K}$ term to generate a new $\mathbf{K}$ term in order to derive the sine and cosine components of the solution, as shown below:

$$\begin{cases} \mathbf{U}^{\mathrm{s}} = \left[\mathbf{K} - \omega^2 \mathbf{M} + \omega^2 \mathbf{C}\left(\mathbf{K} - \omega^2 \mathbf{M}\right)^{-1} \mathbf{C}\right]^{-1} \left[\mathbf{K}' + \omega^2 \mathbf{C}\left(\mathbf{K} - \omega^2 \mathbf{M}\right)^{-1} \mathbf{C}'\right] \mathbf{E}^{\mathrm{s}} \\ \mathbf{U}^{\mathrm{c}} = \left[\mathbf{K} - \omega^2 \mathbf{M} + \omega^2 \mathbf{C}\left(\mathbf{K} - \omega^2 \mathbf{M}\right)^{-1} \mathbf{C}\right]^{-1} \left[\omega \mathbf{C}' - \omega \mathbf{C}\left(\mathbf{K} - \omega^2 \mathbf{M}\right)^{-1} \mathbf{K}'\right] \mathbf{E}^{\mathrm{s}} \end{cases} \tag{39}$$

where $\mathbf{M}$, $\mathbf{C}$, $\mathbf{K}$ represent the mass, damping and total stiffness matrices, respectively, and $\mathbf{C}'$, $\mathbf{K}'$ represent the damping and stiffness matrices of gear transmission errors, respectively.

4.2. Comparison of Analytical and Numerical Solutions

According to the transmission system's vibration differential equation, the vibration displacement and speed response obtained by the numerical solution can be substituted into Formula (24) to obtain the speed and acceleration time domain response curves, as depicted in Figure 12. Take the input speed $n = 500$ r/min, the excitation $T_{at} = 0$ N · m, ignore the torque fluctuation and backlash, transmission error $E = 10$ μm. Comparing the response curves generated by the numerical approach and analytical method yields the comparative time domain curves depicted in Figure 13.

Figure 13 demonstrates that the radial and axial vibration velocity curves of the external gear derived using the harmonic balance approach and the numerical method are largely identical. Consistent results can increase confidence in the system's performance and provide guidance for further research and application. However, it is important to note that both theoretical analysis and numerical simulations have their limitations, and the consistency of results does not imply absolute accuracy. Therefore, further experimental validation and practical application are also necessary.

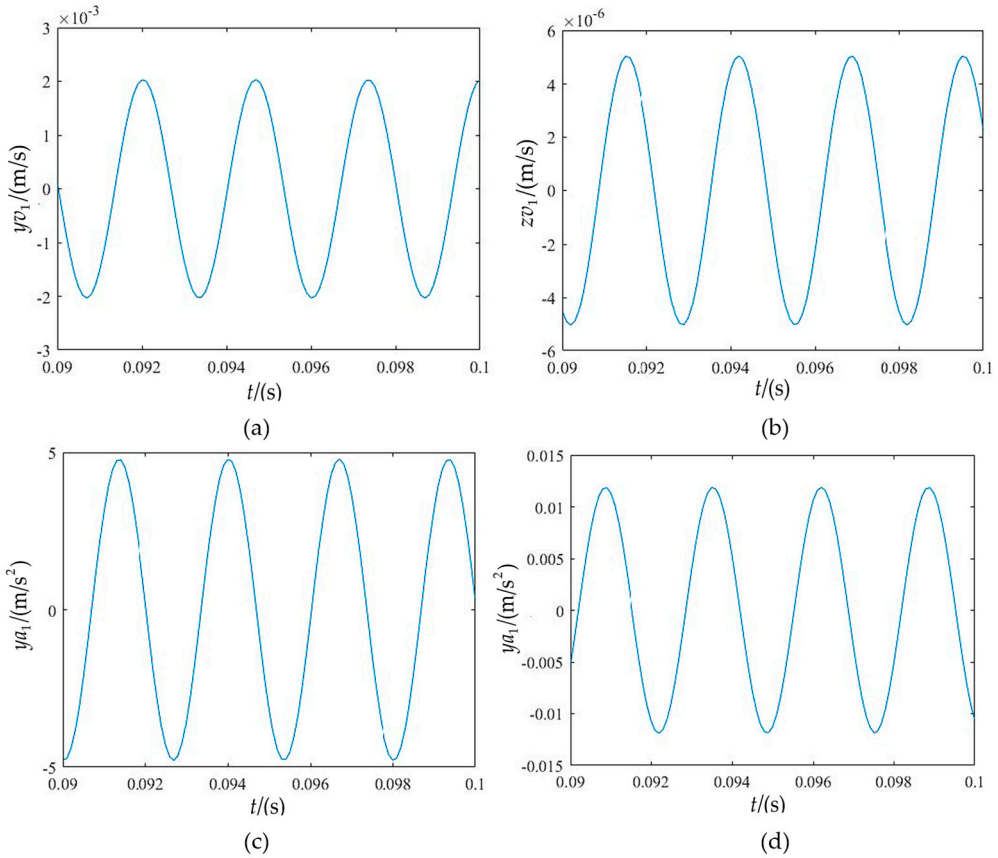


Figure 12. Time domain diagram of gear speed and acceleration based on harmonic balance (**a**,**b**) the radial and axial speed of internal gear; (**c**,**d**) radial and axial acceleration of internal gear.

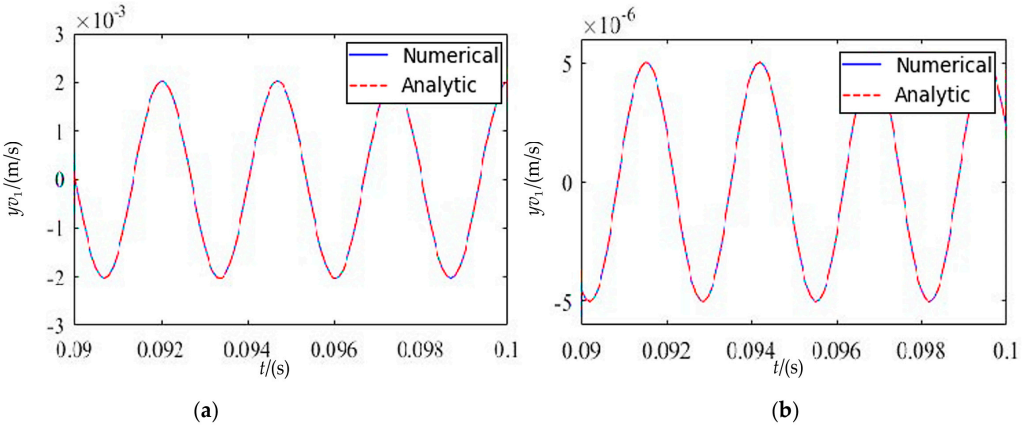


Figure 13. Velocity comparison of numerical solution and analytical solution time domain diagram (**a**,**b**) radial and axial vibration velocity comparison.

Considering that the influence of bearing backlash is ignored at this time, and the clearance functions of both are represented by first−order fitting, there is a certain gap compared with the actual situation. Considering that the analytical method generally fits the backlash function with a polynomial function, the higher the fitting order, the greater the precision. When the harmonic balance method is used to solve the problem, it is found that when the gap function is considered in the numerical solution, the scanning curves of the two have a certain difference. When the backlash is small, the vibration and amplitude of the two are basically the same, and the error is small; when there is a backlash gap, the numerical solution is quite different from the equivalent analytical solution of first−order processing.

For the general harmonic method, if you want to obtain a more accurate solution, you need to increase the equivalent order of the approximate solution and fit the gap function to a higher−order series, which leads to a great increase in the difficulty of solving the harmonic method. Therefore, it is difficult to solve the harmonic method when it is necessary to analyze the characteristic influence caused by the gear backlash with high precision.

5. Conclusions

This paper primarily explores the nonlinear vibration characteristics of parallel−axis internal beveloid gears under external factors such as input torque, rotational fluctuation, and input speed, as well as internal factors such as bearing backlash and tooth backlash. By investigating the impact and role of parameter excitation on the nonlinear vibration characteristics of the transmission system under the combined influence of internal and excitations, it aims to provide references for the structural design optimization and reduction in vibration noise in internal beveloid gear transmission systems. The main achievements and research findings obtained through analysis are as follows:

(1) By utilizing the Runge–Kutta method, the gear dynamic differential equations can be solved to investigate the effects of various parameters on the vibration characteristics of the system. Research shows that: when the input torque changes with a tiny amplitude, it mostly influences the peak value of the system's steady vibration response and has a significant effect on the axial vibration amplitude of the gear; torque fluctuation will increase the instability of the system vibration, and its influence degree is closely related to the input torque amplitude; the input rotational speed of the transmission system directly determines its meshing angular frequency; the increase in its rotational speed under the non−resonant low rotational speed will increase the vibration amplitude rapidly, and when it is close to the natural frequency, there will be a sudden vibration change, which will affect the stability of the transmission system; the bearing backlash is one of the nonlinear parameters, which will affect the vibration stability of the system and the offset of the gear vibration balance position, which will make the gear vibration balance point shift greatly; and the existence of tooth backlash makes the vibration amplitude and stability of the system change, and the beveloid gear can adjust the tooth backlash to a certain extent.

(2) The harmonic balance method is used to calculate and analyze the vibration differential equation of the single−stage internal gear, and the approximate analytical solution of the gear transmission system and the corresponding vibration speed and acceleration time domain response curve are obtained. It is compared with the time domain response curve of vibration velocity obtained by numerical method, and the two are consistent. The sweep curve is drawn to analyze the main and harmonic resonance phenomena of the system, the difference between the linear and nonlinear sweep curves is compared, and the influence of damping on the resonance characteristics is analyzed. It is found that the meshing damping has a strong inhibitory effect on the amplitude of harmonic resonance.

This article has undertaken a certain level of investigation into the vibration characteristics of internal beveloid gear transmission systems. Nevertheless, there are aspects that can still be further enhanced. The distinction between radial and axial backlash of the bearing was not considered in this study, and the influences of factors such as gear eccentricity and lubrication were not taken into account in the dynamic model. Furthermore, in the investigation of the relationship between changes in gear parameters and the improvement of system vibration characteristics, the methods of gear modification to enhance gear vibration characteristics were not considered.

Author Contributions: J.W. conceived and designed the study, and wrote the article. C.F. conducted data extraction and performed the analyses. J.W. applied for the funding which financially supported the study. B.Y. and H.Z. provided their comments and suggestions during discussions and by writing, especially on the data extraction method and paper formatting. All authors have read and agreed to the published version of the manuscript.

Funding: This work is supported by the National Natural Science Foundation of China under Grant Nos. 52075116 and 52175082, and the Natural Science Foundation of Shandong Province under Grant No. ZR2021ME025.

Institutional Review Board Statement: Not applicable.

Informed Consent Statement: Not applicable.

Data Availability Statement: The data presented in this study are available on request from the corresponding author. The data are not publicly available due to privacy.

Conflicts of Interest: The authors declare that they have no known competing financial interest or personal relationship that could have appeared to influence the work reported in this paper.

References

1. Wang, L.J.; Huang, Q.-S.; Zou, W. Research on the summarization of the gear development. *Mech. Res. Appl.* **2008**, *21*, 17–18.
2. Do, T.P.; Ziegler, P.; Eberhard, P. Review on contact simulation of beveloid and cycloid gears and application of a modern approach to treat deformations. *Math. Comput. Model. Dyn. Syst.* **2015**, *21*, 359–388. [CrossRef]
3. Wu, J.-F.; Li, G.-X.; Wang, Q.-H.; Zhuang, S.; Li, H.-M. The backlash analysis and calculation on beveloid gear RV reducer used in robot. *Mach. Des.* **2000**, *3*, 24–26.
4. Ren−Chao, G.E.; Zhang, M.; Dai, G.-H.; Zhang, Z.-B. Analysis of vibration and noise reduction technology of ship gear transmission. *Ship Sci. Technol.* **2018**, *40*, 114–118.
5. Purkiss, S.C. Conical involute gears. *Machinery* **1956**, *89*, 1465–1467.
6. Mitome, K. Table sliding taper hobbing of conical gear using cylindrical hob. Part 1: Theoretical analysis of table sliding taper hobbing. *J. Eng. Ind.* **1981**, *103*, 446–451. [CrossRef]
7. Mitome, K. Table sliding taper hobbing of conical gear using cylindrical hob. Part 2: Hobbing of conical involute gear. *J. Eng. Ind.* **1981**, *102*, 452–455. [CrossRef]
8. Zhao, J.-J.; Huang, J.-L.; Wen, J.-M.; Bian, Y.-H.; Sun, J.-H. Gear Hobbing of Space Beveloid Gears. *Coal Mine Mach.* **2014**, *35*, 135–137.
9. Wu, J.-F.; Li, G.-X. A New Slotting Technology for a Pair of Inside Engaged Gears. *J. Xi'an Pet. Inst.* **2000**, *15*, 45–48.
10. Chen, Q.; Song, C.; Zhu, C.; Du, X.; Ni, G. Manufacturing and contact characteristics analysis of internal straight beveloid gear pair. *Mech. Mach. Theory* **2017**, *114*, 60–73. [CrossRef]
11. Han, J.; Li, D.; Tian, X.; Xia, L. Meshing Principle and Transmission Analysis of a Beveloid Non−circular Gear. In *Advances in Mechanical Engineering*; Sage Publications Inc.: Thousand Oaks, CA, USA, 2020; Volume 12.
12. Cao, B.; Li, G.L.; Fortunato, A.; Ni, H.X. Continuous generating grinding method for beveloid gears and analysis of grinding characteristics. *Adv. Manuf.* **2022**, *10*, 459–478. [CrossRef]
13. Tuplin, W.A. Gear—tooth stresses at high speed. *Proc. Inst. Mech. Eng.* **1950**, *163*, 162–175. [CrossRef]
14. Tuplin, W.A. Dynamic loads on gear teeth. *Mach. Des.* **1953**, *25*, 203.
15. Wang, X.-S.; Wu, S.-J.; Zhou, X.-H.; Hu, J.-C. Nonlinear dynamics analysis of gear transmission system with wear fault. *J. Vib. Shock.* **2013**, *32*, 37–43.
16. Xiang, L.; Gao, N.; Hu, A. Dynamic analysis of a planetary gear system with multiple nonlinear parameters. *J. Comput. Appl. Math.* **2018**, *327*, 325–340. [CrossRef]
17. Jiang, H.; Shao, Y.; Mechefske, C.K. Dynamic characteristics of helical gears under sliding friction with spalling defect. *Eng. Fail. Anal.* **2014**, *39*, 92–107. [CrossRef]
18. Yang, Y.; Xu, M.; Du, Y.; Zhao, P.; Dai, Y. Dynamic analysis of nonlinear time−varying spur gear system subjected to multi−frequency excitation. *J. Vib. Control.* **2019**, *25*, 1210–1226. [CrossRef]
19. Bahk, C.J.; Parker, R.G. Analytical solution for the nonlinear dynamics of planetary gears. *J. Comput. Nonlinear Dyn.* **2011**, *6*, 021007. [CrossRef]
20. Yu, G.; Mao, H.; Jiang, L.; Liu, W.; Valerii, T. Fractal contact mechanics model for the rough surface of a Beveloid gear with elliptical asperities. *Appl. Sci.* **2022**, *12*, 4071. [CrossRef]
21. Sun, R.; Song, C.; Zhu, C.; Wang, Y.; Yang, X. Computational studies on mesh stiffness of paralleled helical beveloid gear pair. *Int. J. Precis. Eng. Manuf.* **2021**, *22*, 123–137. [CrossRef]
22. Sun, R.; Song, C.; Zhu, C.; Yang, X.; Li, X. Computational study of pitting defect influence on mesh stiffness for straight beveloid gear. *Eng. Fail. Anal.* **2021**, *119*, 104971. [CrossRef]

Disclaimer/Publisher's Note: The statements, opinions and data contained in all publications are solely those of the individual author(s) and contributor(s) and not of MDPI and/or the editor(s). MDPI and/or the editor(s) disclaim responsibility for any injury to people or property resulting from any ideas, methods, instructions or products referred to in the content.